Three Dimensional Palmprint Recognition

Wei Li

Institute of Image Processing and Pattern Recognition
Shanghai Jiao Tong University
Shanghai, China
liweistorm@sjtu.edu.cn

Lei Zhang and David Zhang

Biometrics Research Center, Dept. of Computing
The Hong Kong Polytechnic University
Hong Kong, China
(cslzhang, csdzhang)@comp.polyu.edu.hk

Abstract—**Palmprint has been widely studied as its high accuracy and low cost. Most of the previous studies are based on two dimensional (2D) image of the palmprint. However, 2D image can be easily forged, which will threaten the security of palmprint authentication system. Furthermore, 2D image can be easily affected by noise, such as scrabbling and dirty in the palm. To overcome these shortcomings, we develop a three dimensional (3D) palmprint identification system. The structured-light imaging technology is adopted to collect the 3D palmprint data, from which the stable Mean Curvature Image (MCI) is extracted. Then the Competitive Coding (CompCode) technique is used to code the 3D palmprint pattern according the MCI. By using score level fusion of MCI and its CompCode, promising recognition performance is achieved on our established 3D palmprint database.**

Keywords—**3D palmprint identification, biometrics, mean curvature, feature coding**

I.   INTRODUCTION

Automatic personal authentication using biometric information is playing a more and more important role in applications of public security, access control, forensic, banking, etc. Many kinds of biometric authentication techniques have been developed based on different biometric characteristics, which can be generalized into two classes: physiological-based (such as fingerprint, face, iris, palmprint, hand shape, etc.) and behavioral-based (such as signature, voice, gait, etc.) characteristics. Palmprint has been widely studied in the past decade and it has proven to be a unique biometric identifier. Palmprint systems have merits of high accuracy, low cost, user friendliness, etc. However, most of the palmprint recognition techniques are based on the two dimensional (2D) palm images, despite the fact that the human palm is a three dimensional (3D) surface. Although 2D palmprint recognition techniques can achieve high accuracy, the 2D palmprint can be easily counterfeited and much 3D palm structural information is lost. Therefore, it is of high interest to explore new palmprint recognition techniques.

Recently, 3D techniques have been applied to biometric authentication, such as 3D face [1] and 3D ear recognition [2]. Range data are usually used in these 3D biometric applications. Most of the existing commercial 3D scanners use laser triangulation to acquire the 3D depth information. Nonetheless, the laser triangulation based 3D imaging technique has some shortcomings for the biometric application. For example, the resolution of 3D cloud points may not be high enough for the

accuracy requirement in biometric authentication; if we want to improve the data resolution, the laser scanning speed must be decreased and the requirement of real-time authentication is hard to meet.

With the above considerations, we propose to use structured-light imaging [3] to establish the 3D palmprint data acquisition system. The structured-light imaging is able to accurately measure the 3D surface of an object but use less time than laser scanning. In the developed system, when the user put his/her palm on the system, an LED projector will generate structured light stripes and project them to the palm. A series of grey level images of the palm with the stripes on it are captured by a CCD camera, and then the depth information of the palm surface is reconstructed from the stripe images.

As shown in our previous work [4], mean curvature is a stable and valuable feature of the 3D palmprint. By normalizing and mapping the mean curvature value to a plane, we can get a Mean Curvature Image (MCI) which can be used for matching. Meanwhile, Competitive Coding (CompCode) [5] is a very efficient method for 2D palmprint identification. However, it's hard to be extended to 3D palmprint directly because the 3D Gabor filter is not easy to be designed and implemented for the 3D palmprint data. The MCI can well represent 3D palmprint information on the 2D plane, which makes it suitable to introduce the Competitive Coding method into 3D palmprint recognition. By fusing the MCI and Competitive Code results on the matching score level, we can achieve much better performance than any single one of them. A 3D palmprint database with 8000 samples from 200 people is established and a series of experiments are conducted to evaluate the performance of the proposed scheme.

The rest of the paper is organized as follows. Section II describes the acquisition of 3D palmprint data. Section III discusses the ROI region determination and the 3D feature extraction from 3D palmprint. Section IV gives the feature matching methods. Section V presents the experimental results and Section VI concludes the paper.

II.   3D PALMPRINT DATA ACQUISITION

The commonly used 3D imaging techniques include multi-viewpoint reconstruction [6], laser scanning [7] and structured light scanning [3]. Structured-light scanning can measure the object surface in a high accuracy and in a relatively short time period. Considering the requirements of accuracy and speed in

biometric authentication, we choose to use structured-light scanning to acquire the palm depth information.

In structured-light imaging, a light source projects some structured light patterns (stripes) onto the surface of the object. The reflected light is captured by a CCD camera and then a series of images are collected. After some calculation, the 3D surface depth information of the object can be obtained. Fig. 1 illustrates the imaging principle of the structured-light technique [3]. Interested readers can refer to [3] for more details about structured-light imaging. In Fig. 1, there is a reference plane whose height is 0. By projecting light through grating to the object surface, the relative height of a point D at spatial position (x, y) to the reference plane can be calculated as follows [3]

$$h(x, y) = \overline{BD} = \frac{\overline{AC} \cdot \tan \theta_0}{1 + \tan \theta_0 / \tan \theta_n} \qquad (1)$$

with

$$\overline{AC} = \frac{\phi_{CD}}{2\pi} P_0 \qquad (2)$$

where P_0 is the wavelength of the projected light on the reference plane, θ_0 is the projecting angle, θ_n is the angle between the reference plane and the line which passes through the current point and the CCD center, and ϕ_{CD} is the phase difference between points C and D. Because the phase of point D on the 3D object is equal to the phase of point A on the reference plane, ϕ_{CD} can be calculated as:

$$\phi_{CD} = \phi_{CA} = \phi_{OC} - \phi_{OA} \qquad (3)$$

By using (1) and the phase shifting and unwrapping technique [8], we can retrieve the depth information of the object surface by projecting a series of phase stripes on it (13 stripes are used in our system). Some sample patterns of the stripes on the palm are illustrated in Fig. 2.
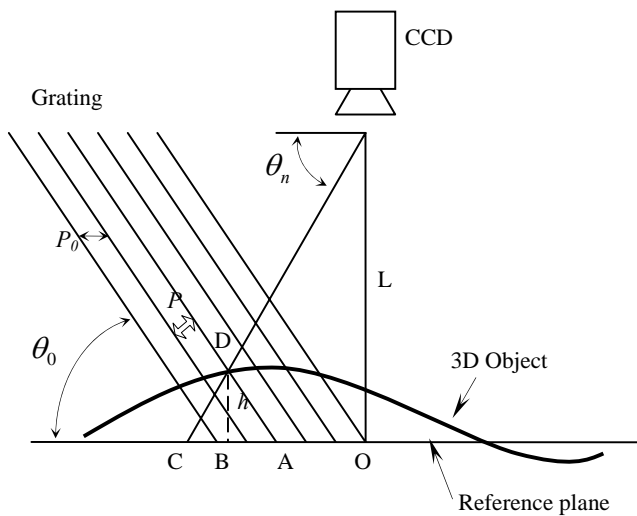

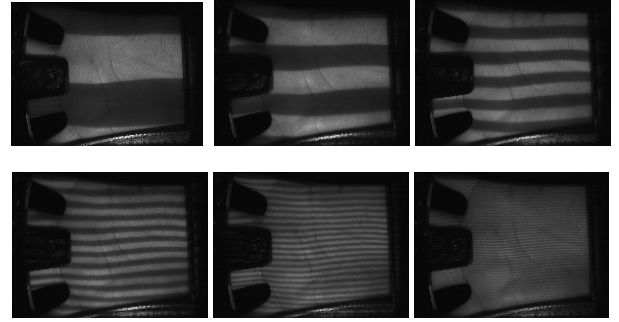Figure 1.   The principle of structured-light imaging.

Figure 2.   Sample patterns of the stripes on the palm.

With the above processing, the relative height of each point, i.e. $h(x,y)$, could be calculated. The range data of the palm surface can then be obtained. In the developed system, the spatial resolution of the 3D image is set as 768×576, i.e. there are totally 442368 cloud points to represent the 3D palmprint information. Fig. 3 shows an example 3D palmprint image captured by the system. The gray level in Fig. 3 is related to the value of $h(x,y)$ and it is rendered by OpenGL automatically for better visualization.

Figure 3.   An example of captured 3D palmprint image.

III.   FEATURE EXTRACTION FROM 3D PALMPRINT

A.   Region of Interest Extraction

From Fig. 3, we can see that in the 3D palmprint image of resolution 768×576, many cloud points, such as those in the boundary area and those in the fingers, could not be used in feature extraction and recognition. Most of the useful and stable features locate in the center area of the palm. In addition, at different times when the user puts his/her hand on the collecting device, there will be some relative displacements of the positions of the palm, even that we impose some constraints on the users to place their hands. Therefore, before feature extraction it is necessary to perform some preprocessing to align the palmprint and extract the central area of it, which is called the Region of Interest (ROI) extraction.

By using the developed structured-light based 3D imaging system, the 2D and 3D palmprint images can be obtained simultaneously, and there is a one-to-one correspondence between the 3D cloud points and the 2D pixels. Therefore, the ROI extraction of the 3D palmprint data can be easily implemented via the 2D palmprint ROI extraction procedure. In this paper, we use the algorithm in [9] to extract the 2D ROI. Once the 2D ROI is extracted, the 3D ROI is obtained by

grouping the cloud points that are in correspondence to the pixels in the 2D ROI. Fig. 4 illustrates the ROI extraction process. Fig. 4a shows a 2D palmprint image, the established local coordinate system by using the algorithm in [9] and the ROI (i.e. the rectangle); Fig. 4b shows the extracted 2D ROI; Fig. 4c shows the 3D palmprint image and Fig. 4d shows the obtained 3D ROI by grouping the cloud points corresponding to the pixels in 2D ROI.
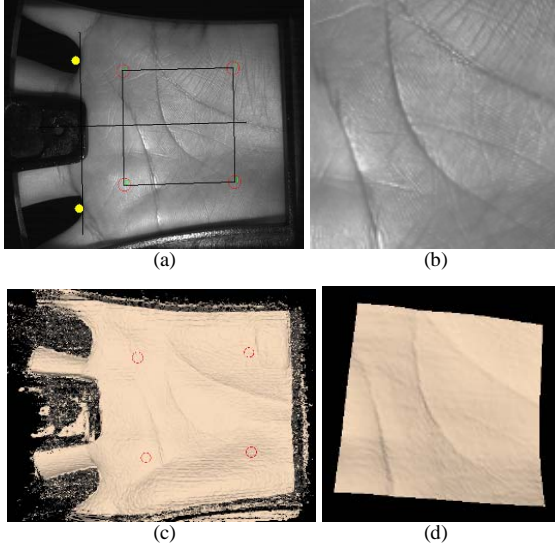

Figure 4. The ROI extraction of 3D palmprint from its 2D counterpart. (a) The 2D palmprint image, the adaptively established coordinate system and the ROI (i.e. the rectangle); (b) the extracted 2D ROI; (c) the 3D palmprint image, whose cloud points have a one-to-one correspondence to the pixels in the 2D counterpart; (d) the obtained 3D ROI by grouping the cloud points corresponding to the pixels in 2D ROI.

By using ROI extraction procedure, the 3D palmprint images are aligned so that the small translation and rotation introduced in the data acquisition process are corrected. In addition, the data amount used in the following feature extraction and matching process is significantly reduced. This will save much computational cost.

B. Curvature Calculation

With the ROI obtained from the original 3D palmprint data, stable and unique features are expected to be extracted for the following pattern matching and recognition. The depth information in the acquired 3D palmprint reflects the relative distance between the reference plane and each point in the object. The z-values of the 3D cloud points are affected by the position of hand in scanning. However, each time the users put their hands, the 3D space locations will be different. The ROI extraction process can only correct, to some extent, the rotation and translation displacements in the x-y plane but not the z-axis. Moreover, the human palm is not a rigid object and it can have some deformation. Those factors introduce much noise in the 3D palmprint cloud points and make the well-known ICP algorithms [10] not suitable for 3D palmprint recognition. Instead, the local invariant features, such as the curvatures of a surface, will be much more stable in representing the characteristics of 3D palmprint.

Let p be a point on the surface S. Consider all curves C_i on S passing through the point p. Each curve C_i will have an associated curvature K_i at p. Among those curvatures K_i, at least one is characterized as maximal k_1 and one as minimal k_2, and these two curvatures k_1 and k_2 are known as the principal curvatures of point p on the surface [11]. The Mean curvature H and the Gaussian curvature K of p are defined as follows

$$H = \frac{1}{2}(k_1 + k_2), \ K = k_1 * k_2 \tag{4}$$

The Mean and Gaussian curvatures are intrinsic measures of a surface, i.e. they depend only on the surface shape but not on the way how the surface is placed in the 3D space [11]. Thus such curvature features are robust to the rotation, translation and even some deformation of the palm. The captured 3D palmprint data are organized range data. We adopt the algorithm in [12] to estimate the Mean and Gaussian curvatures for its simplicity and effectiveness as follows

$$H = \frac{(1+(h_y)^2)h_{xx} - 2h_x h_y h_{xy} + (1+(h_x)^2)h_{yy}}{2(1+(h_x)^2+(h_y)^2)^{3/2}} \tag{5}$$

$$K = \frac{h_{xx}h_{yy} - (h_{xy})^2}{(1+(h_x)^2+(h_y)^2)^2} \tag{6}$$

where h is the height of the points on the palmprint to the reference plane, h_x, h_y, h_{xx}, h_{yy} and h_{xy} are the first, second and hybrid partial derivatives of h to x and y coordinates separately.

With (5) and (6), the Mean and Gaussian curvatures of a 3D palmprint image can be calculated. For better visualization and more efficient computation, we convert the original curvature images into grey level images with integer pixels. We first transform the curvature image C (Gaussian curvature K or Mean curvature H) to $\bar{C}$ as follows

$$\bar{C}(i, j) = 0.5(C(i, j) - \mu)/(4\delta) + 0.5 \tag{7}$$

where μ and δ are the mean and standard deviation of the curvature value. With (7), most of the curvature values will be normalized into the interval [0,1]. We then map $\bar{C}(i, j)$ to an 8-bits grey level image $G(i,j)$:

$$G(i, j) = \begin{cases} 0 & \bar{C}(i, j) \le 0 \\ round\left(255 \times \bar{C}(i, j)\right) & 0 < \bar{C}(i, j) < 1 \\ 255 & \bar{C}(i, j) \ge 1 \end{cases} \tag{8}$$

We call images $G(i,j)$ the Mean Curvature Image (MCI) and Gaussian Curvature Image (GCI), respectively for Mean and Gaussian curvatures. Fig. 5 illustrates the MCI and GCI images of three different palms and Fig. 6 illustrates the MCI and GCI images of a palm at different acquisition times. We can see that the 2D MCI and GCI images can well preserve the 3D palm surface features. Not only the principal lines, which are the most important texture features in palmprint recognition, are clearly enhanced in MCI/GCI, but also the depth information of different shape structures is well preserved.
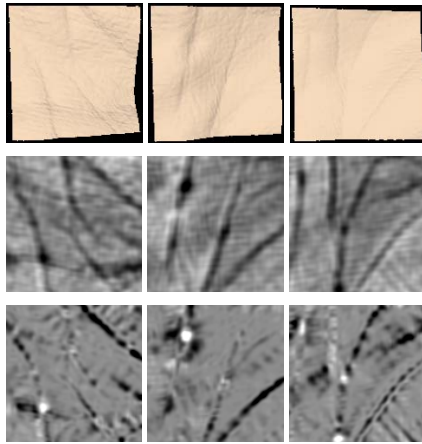
Figure 5. The 3D ROI images (first row) of three different palmprints and their MCI (second row) and GCI (third row) images. From left to right, each column shows the images of one palm, respectively.
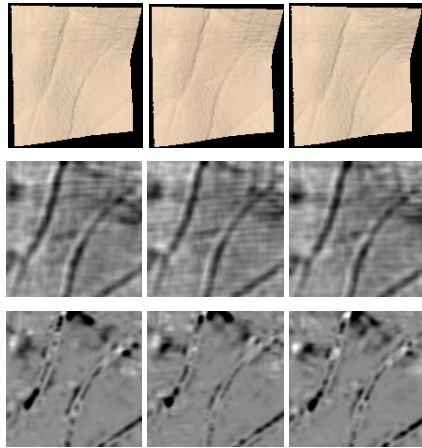

Figure 6. The 3D ROI images (first row) of the same palmprint but collected at different times and their MCI (second row) and GCI (third row) images. From left to right, each column shows the images for each time, respectively.

C. Competitive Coding

There are plenty of directional and structural information on palmprint which can be used for identity identification. The Gabor filters, which are derived from harmonic functions multiplied by Gaussian functions, have excellent ability to extract these features. By using several Gabor filters with different directions to convolute the image, the direction along which the Gabor filter has the greatest response can be set as the direction of that point in the image. The directional features can then be matched by angular distance for identification. This process is called the Competitive Coding scheme [5]. In this paper, the following Gabor filter is used for extracting the directions [13]:

$$\psi(x, y, \omega, \theta) = \frac{\omega}{\sqrt{2\pi}\kappa} e^{-\frac{\omega^2}{8\kappa^2}(4x'^2 + y'^2)} (e^{i\omega x'} - e^{-\frac{\kappa^2}{2}}) \quad (9)$$

where

$$x' = (x - x_0)\cos\theta + (y - y_0)\sin\theta$$

$$y' = -(x - x_0)\sin\theta + (y - y_0)\cos\theta$$

and (x_0, y_0) is the center of the function; ω is the radial frequency in radians per unit length and θ is the orientation of the Gabor functions in radians; and κ is a coefficient defined by

$$\kappa = \sqrt{2\ln 2}\left(\frac{2^\alpha + 1}{2^\alpha - 1}\right) \quad (10)$$

where α is the half-amplitude bandwidth of the frequency response.

Fig. 7 shows the different directional Gabor filter templates used in this paper. Considering the accuracy and efficiency, we choose six different directions

$$\theta = 0, \ \pi/6, \ 2\pi/6, \ 3\pi/6, \ 4\pi/6, \ 5\pi/6$$

respectively. Convolving the six templates with the MCI, and selecting the direction which leads to the greatest response, we get the directional features of MCI as shown in Fig. 8, from which we can see that the extracted directions can well represent the line structure of its neighboring region.
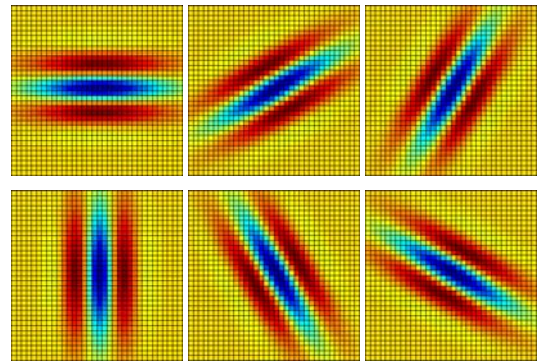

Figure 7. The directional Gabor filter templates used in this paper. From top left to bottom right, $\theta = 0, \ \pi/6, \ 2\pi/6, \ 3\pi/6, \ 4\pi/6, \ 5\pi/6$ respectively.
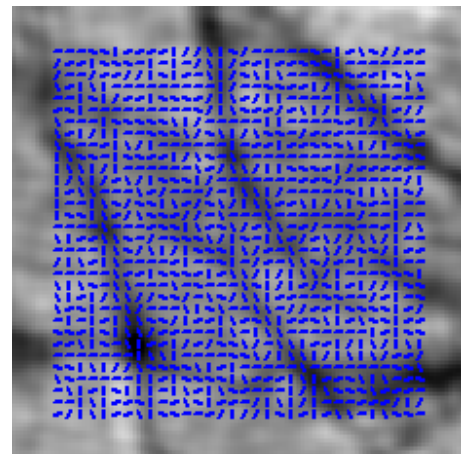

Figure 8. Illustration of directions plotting on MCI.

IV. FEATURE MATCHING

In Section, there are two kinds of features extracted, location and direction, each of which can be used for matching. Apparently, they can also be fused for better results.

A. Location Matching

The principal lines and strong wrinkles are the most stable and significant features in the palmprint. Their locations in the palmprint are important information for matching. With (11) we convert the MCI into binary images, which can then be directly used for matching

$$B(i,j) = \begin{cases} 1 & G(i,j) < c \cdot \mu_G \\ 0 & others \end{cases} \quad (11)$$

where c is a constant and μ_G is the mean value of $G(i,j)$. With our experience, we set $c = 0.7$ in the experiments. Fig. 9 shows the binarized versions of the MCI images in Fig. 5 and Fig. 6.
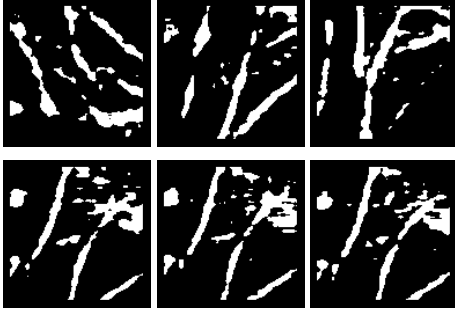

Figure 9. The binarized MCI images. The white areas represent the high mean curvature region position.

We use the AND operation to calculate the matching score of location features. Denote by B_d the binarized MCI image in the database and by B_t the input MCI binary image. Suppose the image size is $n \times m$. The matching score between B_d and B_t is defined as:

$$R_P = \frac{2 \sum_{i=1}^{n} \sum_{j=1}^{m} B_d(i,j) \oplus B_t(i,j)}{\sum_{i=1}^{n} \sum_{j=1}^{m} B_d(i,j) + \sum_{i=1}^{n} \sum_{j=1}^{m} B_t(i,j)} \quad (12)$$

where symbol "$\oplus$" means the AND logic operation.

B. Direction Matching

Denote by integers 0, 1, 2, 3, 4 and 5 the six directions $0, \pi/6, 2\pi/6, 3\pi/6, 4\pi/6, 5\pi/6$ respectively. Intuitively, the distance between parallel directions should be 0, while the distance between perpendicular directions should be 3. In other cases, the distance should be 1 or 2. Let D_d and D_t be the direction sets of the MCI images. The matching score between them can be defined as:

$$R_D = \frac{\sum_{i=1}^{n} \sum_{j=1}^{m} F(D_d(i,j), D_t(i,j))}{3nm} \quad (13)$$

where

$$F(x,y) = \min(|x-y|, 6-|x-y|) \quad (14)$$

C. Score Level Fusion

There are many score level fusion methods, such as Min-score, Max-score, Weight-score, SVM, etc. [14, 15]. Here, we use the Average-score method which is simple but efficient. The fusion of the two scores is then

$$R_F = (R_P + R_D)/2 \quad (15)$$

V. EXPERIMENTAL RESULTS

A 3D palmprint database has been established by using the developed 3D palmprint imaging device. The database contains 8000 samples from 200 volunteers, including 136 males and 64 females. The youngest one is 10 years old and the oldest one is 55 years old. Most of them are students and staff in our institutes. The 3D palmprint samples were collected in two separated sessions, and in each session 10 samples were collected from both the left and right hands of each subject. The average time interval between the two sessions is one month. The original spatial resolution of the data is 768×576. After ROI extraction, the central part (256×256) is used for feature extraction and recognition. The z-value resolution of the data is 32 bits.

We performed two types of experiments on the established database: verification and identification. In verification, the class of the input palmprint is known and each of the 3D samples was matched with all the other 3D samples in the database. A successful matching is called intra-class matching or genuine if the two samples are from the same class. Otherwise, the unsuccessful matching is called inter-class matching or impostor. Using the established database, there are 31,996,000 matchings in total. The verification experiments were performed by using each of the location and direction features, as well as the fusion of them at the score level. The ROC curves are shown in Fig. 10. The EER values are listed in Table I, where the feature extraction and matching time by using different features are also listed.

The experiments of identification were also conducted on the 3D palmprint database. In identification, we do not know the class of the input palmprint but want to identify which class it belongs to. In the experiments we let the first sample of each class in the database be template and use the other samples as probes. Therefore, there are 7600 probes and 400 templates. The probes were matched with all the templates models, and for each probe, the matching results were ordered according to the matching scores. Then we can get the cumulative match curves as shown in Fig. 11. The cumulative matching performance, rank-one recognition rate and lowest rank of perfect recognition (i.e. the lowest rank when the recognition rate reaches 100%) are listed in Table II. From the experimental results we can see that the performance of feature fusion is much better than using any single one of them.
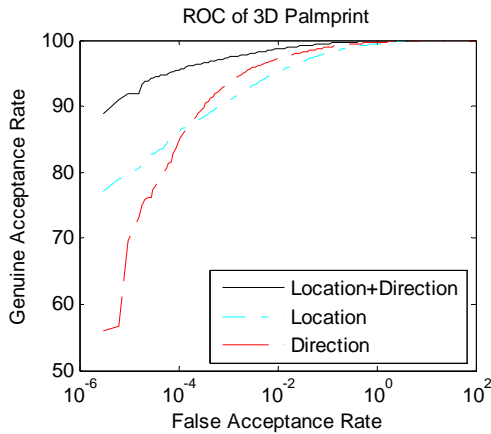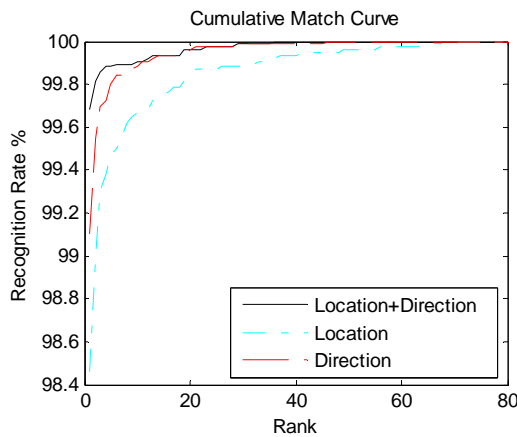
Figure 10. ROC curves by different methods.

Figure 11. CMC curves by different methods.

TABLE I. VERIFICATION PERFORMANCE, FEATURE EXTRACTION TIME AND MATCHING TIME BY DIFFERENT TYPES OF FEATURES

	Location	Direction	Fusion
EER	0.688%	0.495%	0.284%
Feature extraction time	112ms	97ms	209ms
Matching time	0.86ms	0.15ms	1.01ms

TABLE II. IDENTIFICATION PERFORMANCE BY DIFFERENT TYPES OF FEATURES

	Location	Direction	Fusion
Rank-one recognition rate	98.46%	99.11%	99.68%
Lowest rank for perfect recognition	71	46	36

VI. CONCLUSIONS

In this paper, we explored a new technique for palmprint based biometrics: 3D palmprint recognition. First a structured-light based 3D palmprint data acquisition system was developed. After the 3D palmprint image was captured, the region of interest (ROI) was extracted to roughly align the palm and remove the unnecessary cloud points. We then developed the curvature based feature extraction algorithms to obtain the Mean Curvature Image (MCI), Gaussian Curvature Image (GCI) features. We then extracted the location and direction features from MCI. At last, a score level feature fusion strategy of the two types of features was used to classify the palmprints. A 3D palmprint database with 8000 samples from 200 individuals (400 palms) was established, on which a series of verification and identification experiments were performed. The experimental results show that both of the location and direction features of 3D palmprint can achieve high recognition rate and fusing them can get much higher performance. In the future, more advanced and powerful feature extraction and matching techniques are to be developed for a better recognition performance.

REFERENCES

[1] C. Samir, A. Srivastava, and M. Daoudi, "Three-dimensional face recognition using shapes of facial curves," IEEE Trans. on PAMI, vol. 28, no. 11, pp. 1858 - 1863, Nov. 2006.

[2] P. Yan and K. W. Bowyer, "Biometric recognition using 3D ear shape", IEEE Trans. on PAMI, vol. 29, no. 8, pp. 1297-1308, Aug. 2007.

[3] V. Srinivassan and H.C. Liu, "Automated phase measuring profilometry of 3D diffuse object," Appl. Opt., 23(18): 3105-3108, 1984.

[4] D. Zhang, G. Lu, W. Li, L. Zhang, and N. Luo, "Three dimensional palmprint recognition using structured light imaging," IEEE International Conference on Biometrics: Theory, Applications and Systems, pp. 1-6, Sept. 2008.

[5] A.W.K. Kong and D. Zhang, "Competitive coding scheme for palmprint verification," Proceedings of International Conference on Pattern Recognition, vol. 1, pp. 520-523, 2004.

[6] R. Hartley, Multiple View Geometry in Computer Vision, Cambridge, New York: Cambridge University Press, 2000.

[7] F. Blais, M. Rious, and J.A. Beraldin, "Practical considerations for a design of a high precision 3-D laser scanner system," Proc. SPIE, vol. 959, pp. 225-246, 1988.

[8] H.O. Saldner and J.M. Huntley, "Temporal phase unwrapping: application to surface profiling of discontinuous objects," Appl.Opt., 36(13):2770-2775, 1997.

[9] D. Zhang, A.W.K. Kong, J. You, and M. Wong, "On-line palmprint identification," IEEE Trans. on PAMI, vol. 25, no. 9, pp. 1041-1050, 2003.

[10] P. J. Besl and N.D. McKay, "A method for registration of 3-D shapes," IEEE Trans. on PAMI, vol. 14, no. 2, pp. 239 - 256, Feb. 1992.

[11] W. Kühnel, Differential Geometry: Curves-Surfaces-Manifolds, American Mathematical Society, 2006.

[12] P.J. Besl and R.C. Jain, "Segmentation through variable-order surface fitting," IEEE Trans. on PAMI, vol. 10, no. 2, pp. 167 - 192, March 1988.

[13] T.S. Lee, "Image representation using 2D Gabor wavelet," IEEE Trans. on PAMI, vol. 18, no. 10, pp. 959-971, 1996.

[14] R. Snelick, U. Uludag, A. Mink, M. Indovina, and A. Jain, "Large-scale evaluation of multimodal biometric authentication using state-of-the-art systems," IEEE Trans. on PAMI, vol. 27, no. 3, pp. 450- 455, March 2005.

[15] V. Vapnik, The Nature of Statistical Learning Theory, Springer-Verlag, New York, 1995.